

Femtosecond dynamics of Cu(CD₃OD)

Jack Barbera

JILA, University of Colorado, Boulder, Colorado 80309 and Department of Chemistry and Biochemistry, University of Colorado, Boulder, Colorado 80309

Samantha Horvath

Department of Chemistry, The Ohio State University, Columbus, Ohio 43210

Vladimir Dribinski

JILA, University of Colorado, Boulder, Colorado 80309; Department of Chemistry and Biochemistry, University of Colorado, Boulder, Colorado 80309; and KLA-Tencor Corporation, San Jose, California 95134

Anne B. McCoy

Department of Chemistry, The Ohio State University, Columbus, Ohio 43210

W. Carl Lineberger

JILA, University of Colorado, Boulder, Colorado 80309 and Department of Chemistry and Biochemistry, University of Colorado, Boulder, Colorado 80309

(Received 1 December 2006; accepted 9 January 2007; published online 27 February 2007)

We report the femtosecond nuclear dynamics of Cu(CD₃OD) van der Waals clusters, investigated using photodetachment-photoionization spectroscopy. Photodetachment of an electron from Cu⁻(CD₃OD) with a 150 fs, 398 nm laser pulse produces a vibrationally excited neutral complex that undergoes ligand reorientation and dissociation. The dynamics of Cu(CD₃OD) on the neutral surface is interrogated by delayed femtosecond resonant two-photon ionization. Analysis of the resulting time-dependent signals indicates that the nascent Cu(CD₃OD) complex dissociates on two distinct time scales of 3 and 30 ps. To understand the origins of the observed time scales, complimentary studies were performed. These included measurement of the photoelectron spectrum of Cu⁻(CD₃OD) as well as a series of calculations of the structure and the electronic and vibrational energies of the anion and neutral complexes. Based on the comparisons of the experimental and calculated results for Cu(CD₃OD) with those obtained from earlier studies of Cu(H₂O), we conclude that the 3 ps time scale reflects the energy transfer from the rotation of CD₃OD in the complex to the dissociation coordinate, while the 30 ps time scale reflects the energy transfer from the excited methyl torsion states to the dissociation coordinate. © 2007 American Institute of Physics. [DOI: 10.1063/1.2464103]

I. INTRODUCTION

Spectroscopy is a powerful tool in the investigation of many chemical phenomena. Combined with gas-phase complexes, spectroscopy has been used to probe the nature of solvation in charged solvent-solute systems.¹⁻⁸ Dynamics occurring within these systems upon solute excitation⁹⁻¹³ can be difficult to characterize due to the large number of interacting species and the rapid changes in their configurations. Size selection of gas-phase solvent-solute complexes allows for detailed dynamical investigations of individual solvent perturbations on the solute.^{12,14-19} In this study we use time-resolved pump-probe laser spectroscopy to examine the dissociation dynamics initiated upon electron photodetachment of Cu⁻(CD₃OD). Our group used similar pump-probe techniques to examine the dynamics of Cu⁻(H₂O)_{*n*},^{20,21} and such anion-water complexes have been the subject of numerous theoretical and experimental investigations.^{3,4,22-31} Of particular relevance to this work are a very recent investigation of Na(H₂O) classical dynamics by Kondo *et al.*³² and an investigation of the infrared spectra of coinage metal anion-water complexes by Schneider *et al.*⁵

In previous studies of Cu⁻(H₂O),^{20,33} electron photodetachment was shown to lead to large-amplitude H₂O reorientation within and dissociation from Cu(H₂O), due to the difference in topology between the anion and neutral potential energy surfaces. The Cu⁻(H₂O) complex has a hydrogen-bonded, Cu⁻-HOH, minimum energy configuration, while in neutral Cu(H₂O) the stronger Cu-O interaction determines its minimum energy configuration. Electron photodetachment from Cu⁻(H₂O) produces an ensemble of vibrationally excited Cu(H₂O) complexes with an average internal energy near the dissociation threshold of the complex. For the Cu(H₂O) study, following electron photodetachment from Cu⁻-HOH, dissociation of Cu(H₂O) occurred on three different time scales, each separated by an order of magnitude. Some 30% of the nascent Cu(H₂O) complexes directly dissociated. The remaining bound complexes dissociated on a 10 ps time scale via coupling of H₂O rotation to the Cu-H₂O dissociation coordinate and on a 100 ps time scale by coupling of the H₂O intramolecular bending vibration with the Cu-H₂O dissociation coordinate.^{20,33,34}

Hydrogen and methyl substituents, and functional groups in general, play pivotal roles in a wide array of

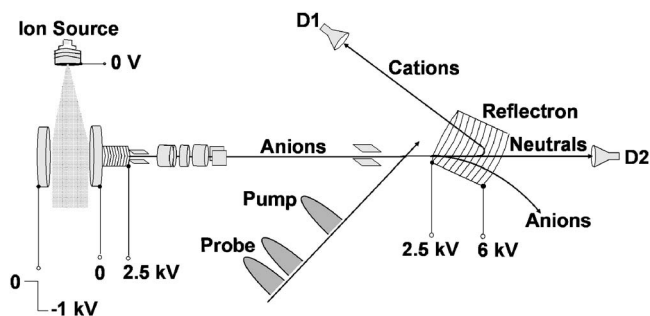


FIG. 1. Schematic diagram of the photodetachment-photoionization apparatus.

chemical reactions. Substitutions of CH_3 for H, and vice versa, can influence reactivity, especially due to steric interactions. Methyl groups have been shown to affect the structure and binding energy in $\text{I}^-(\text{ROH})$ complexes ($\text{R}=\text{H}, \text{CH}_3$),³⁵ and have recently been part of an investigation of infrared spectral features in $\text{Cl}^-(\text{ROH})$ complexes, ($\text{R}=\text{H}, \text{CH}_3, \text{CH}_3\text{CH}_2$).³⁶ In this paper we report on the effects of a methyl group addition on the dissociation dynamics of a metal-ligand complex. We are interested in determining how the methyl group affects the solvent reorientation and dissociation dynamics in a $\text{Cu}^-(\text{ROH})$ complex ($\text{R}=\text{H}, \text{CH}_3$). For experimental reasons, we carry out our spectroscopic studies using fully deuterated methanol. Reports from previous investigations^{20,21} on $\text{Cu}^-(\text{H}_2\text{O})_n$ show no significant difference in the time evolution of the dissociating neutral complexes upon deuteration.

We structure the remainder of this paper as follows. Section II describes the experimental apparatus and techniques. In Sec. III, we describe the details of the *ab initio* electronic structure calculations and vibrational wave function determination. Section IV presents the results and discussion of our experimental and theoretical work in light of the previous $\text{Cu}(\text{H}_2\text{O})$ results. Finally, in Sec. V, we summarize our conclusions.

II. EXPERIMENT

The charge-reversal instrument used to study the time-resolved photodetachment-photoionization of $\text{Cu}^-(\text{CD}_3\text{OD})$ has been described previously.^{20,21,37} Briefly, cluster anions are produced and injected into a tandem time-of-flight mass spectrometer where the cationic photoproducts are monitored as a function of pump-probe delay time. A schematic diagram of the charge-reversal instrument is presented in Fig. 1.

A. Ion production, transport, and product analysis

We produce the metal-ligand clusters via a high-pressure pulsed sputtering discharge ion source. A carrier gas, a mixture consisting of 80% Ne and 20% Ar at stagnation pressures between 6 and 8 atm, flows through a small stainless steel vial containing liquid methanol- d_4 (CD_3OD , Aldrich, CAS No. 811-98-3) at room temperature and is expanded into vacuum through a pulsed (200 Hz) general valve (0.8 mm orifice). Copper anions are produced when the carrier gas flows past a 1 mm gap between a copper rod cathode maintained at -2 – 3 kV and a stainless steel anode main-

tained at ground. Immediately following the discharge, cluster anions form in the expanding gas. The gas enters a 40° cone used to cool and stabilize clusters upon introduction into the $\sim 5 \times 10^{-5}$ Torr pressure of the source chamber. Along with $\text{Cu}^-(\text{CD}_3\text{OD})_n$ ions, the source generates Cu_n^- , $\text{Cu}^-(\text{D}_2\text{O})_n$, Cu^-D_n , Cu^-OD , $\text{Cu}^-(\text{CD}_3\text{O})$, and $\text{CD}_3\text{O}^-(\text{CD}_3\text{OD})_n$ anions. In order to avoid mass contamination of $^{63}\text{Cu}^-(\text{CD}_3\text{OD})$ with $^{65}\text{Cu}^-(\text{CD}_3\text{O})$, we study the less abundant, but isotopically pure, m/z 101 ion packet, $^{65}\text{Cu}^-(\text{CD}_3\text{OD})$. We did not carry out the photodetachment-photoionization experiments on $^{65}\text{Cu}^-(\text{CH}_3\text{OH})$ due to the congestion of the mass spectrum in that region.

While evaporative cooling^{3,38} allows estimates of anion cluster temperatures, rotational and vibrational temperatures of the anions produced in our sputtering discharge source have not been well characterized. Previous anion cluster studies estimate the temperature of $(\text{H}_2\text{O})_{18}^-$ and $\text{I}_2^-(\text{CO}_2)_{16}$ cluster ions^{39,40} and indicate that these cluster temperatures are ~ 150 and ~ 50 K, respectively. We use these studies to estimate the temperature for our smaller $\text{Cu}^-(\text{CD}_3\text{OD})$ clusters to be greater than 150 K. For the purpose of calculations in this study, we use a vibrational temperature of 200 K. The qualitative conclusions, however, do not depend on the exact temperature.

Negative ions are extracted into a differentially pumped Wiley-McLaren⁴¹ time-of-flight mass spectrometer by a pulsed transverse electric field located 10 cm below the expansion nozzle. Further acceleration to 3.5 keV brings ions to a spatial and temporal focus at the photodetachment region, 1.8 m downstream. After the laser interaction region, neutral clusters, produced via photodetachment, are detected on an in-line channeltron detector. Cation photoproducts, produced upon ionization of the neutral clusters, enter a reflectron mass spectrometer and are subsequently counted with an off-axis microchannel plate detector. The remaining anions are deflected away from the detectors. Fluctuation effects in the negative ion intensity and flight time are reduced by normalization of the time-dependent cation signal with the time-independent neutral signal.

B. Laser system

The femtosecond laser system used for the photodetachment-photoionization experiments is essentially the one employed in earlier studies.^{20,37,42} Briefly, a Ti:sapphire oscillator produces ~ 85 fs pulses at ~ 796 nm, which are amplified to 3 mJ/pulse (120 fs) at 400 Hz by a regenerative, multipass Ti:sapphire amplifier. The amplified pulses are used to generate second harmonic (398 nm) and third harmonic (265 nm) radiations, as well as to pump an optical parametric amplifier (OPA), whose fourth harmonic output provides tunable radiation. For this study the OPA is tuned to 327 nm, the frequency of the $\text{Cu } ^2P_{1/2} \leftarrow ^2S_{1/2}$ resonance transition. The 398 and 327 nm pulses pass through delay stages and are further combined with the 265 nm pulse in a collinear configuration. All three pulses are focused to a spot of ~ 1 mm diameter at the point of interaction with the ion packet, where their typical energies are 100 μJ for 398 nm, 10 μJ for 327 nm, and 60 μJ for 265 nm.

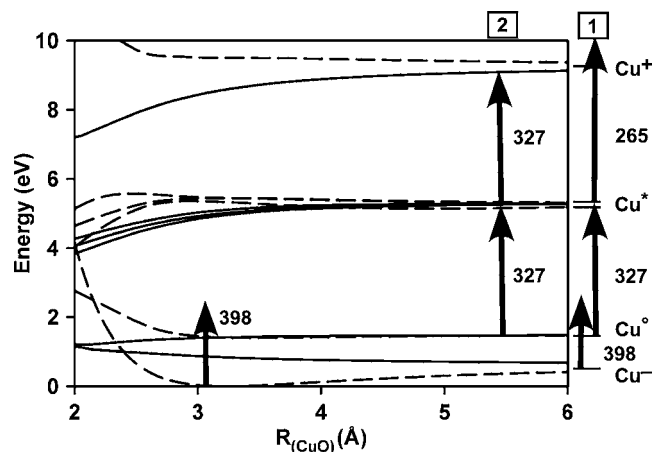


FIG. 2. Potential energy curves, plotted as functions of the Cu–O distance R , along with laser pump-probe schemes. The dashed curves represent cuts in the hydrogen-bonded orientation, while the solid curves represent the orientation in which the copper atom is closest to the oxygen atom. The vertical arrows represent various pump-probe processes employed in the experiments reported here.

Zero delay time between the pump and probe pulses is found *in situ* using three-color, three-photon photodetachment-photoionization of Cu⁻. A 398 nm photon photodetaches an electron from Cu⁻, and a sequence of 327 and 265 nm photons resonantly ionizes the ²S_{1/2} Cu atom through the ²P_{1/2} intermediate state. A fixed delay of 0.3 ps is set between the excitation (327 nm) and ionization (265 nm) pulses to maintain photon sequence during day-to-day alignment; this delay does not affect the cation intensity or the neutral dynamics. As the photodetachment-resonant photoionization delay time (Δt) is varied, the Cu⁺ signal exhibits a step function increase at $\Delta t=0$. From fitting the time dependence of this step to a tanh function, we determine the time resolution of the experiments to be 260 fs.

C. Experimental details and data acquisition

The potential energy curves, plotted as functions of the Cu–O distance in Fig. 2, show that neutral Cu(CD₃OD) complexes are formed by electron photodetachment from Cu⁻(CD₃OD) using a 398 nm pulse. Monitoring the time evolution of the neutral cluster is accomplished by photoionizing Cu(CD₃OD) and its fragments in various pump-probe schemes. Figure 2 shows the two different pump-probe schemes used to detect the cation photoproducts. Scheme 1 in Fig. 2 is used to monitor the Cu⁺ evolution as a function of the delay between the photodetachment and the excitation/ionization pulses; similarly, scheme 2 in Fig. 2 is used to monitor the Cu⁺(CD₃OD) evolution. Typical Cu⁺(CD₃OD) and Cu⁺ signals are ~ 0.5 cations per laser shot.

Individual Cu⁺ and Cu⁺(CD₃OD) product signals are acquired by scanning a range of pump and probe time delays. A single scan entails an accumulation of 800 laser shots at each time delay. To obtain one set of data, an average of $\sim 4 \times 10^4$ laser shots is recorded per individual time delay. The time-dependent cation signal is divided by the neutral signal, and background contributions, arising from individual photodetachment or photoionization pulses alone, are subtracted from the time-dependent signals that depend on both

sets of pulses. The error bars for the experimental data are obtained by averaging multiple data sets, and this averaged cation time dependence is fitted to the functional forms described in Sec. IV B. The standard deviation of the fit provides the reported error. More details are provided in earlier publications.^{20,21}

III. THEORY

Our previous discussion of the dynamics of Cu(H₂O) focused on a three-dimensional, fully coupled treatment that included the three intermolecular degrees of freedom of the complex. Although the full-dimensional treatment gave useful information, we found that many of these insights were borne out in analyses of the three, separate one-dimensional slices. Since calculating Cu(CD₃OD) in full dimensionality is impractical, we draw from our experiences with Cu(H₂O) and expect that the one-dimensional decoupled picture should also hold for Cu(CD₃OD).

The calculations used to characterize the Cu(CD₃OD) complex fall into two general categories. First we determine the minimum energy configurations for the anion, neutral, and cation complexes and then evaluate a series of one-dimensional slices through the potential energy surfaces, starting from these geometries. These one-dimensional potential energy surfaces are used to calculate vibrational wave functions and energies using a sinc-discrete variable representation (DVR).^{43,44} The resulting energies and wave functions are used to investigate the regions of the potential that are sampled by the Cu(CD₃OD) system upon electron photodetachment. In particular, we focus on the partitioning of energy among the internal coordinates and how this is reflected in the time-dependent signal and Cu(CD₃OD) photoelectron spectrum.

A. *Ab initio* calculations

All electronic structure calculations are performed using the GAUSSIAN 98 or GAUSSIAN 03 program packages.^{45,46} The basis sets and level of theory used in these calculations have been described in a previous study.³³ The basis set used to represent the copper atom is an augmented form of the Stuttgart-Dresden-Bonn (SDB) relativistic core potential developed by Dolg *et al.*,⁴⁷ referred to as aug-SDB. The aug-SDB basis was developed by Wang *et al.*⁴⁸ during their investigation of anion and neutral CuX₂ (X=Cl,Br). Hydrogen, oxygen, and carbon are each represented by aug-cc-pVTZ (Refs. 49 and 50) basis sets. Second-order Møller-Plesset perturbation theory (MP2) was used to optimize all geometries as well as in calculations of several potential energy surfaces. The minimum energy configurations for the anion, neutral, and cation complexes are shown in Figs. 3(a)–3(c), respectively.

Both radial and angular one-dimensional potential slices are calculated at the MP2 level of theory, beginning from the minimum energy configuration of the anion and neutral. We also calculated one-dimensional cuts starting from the vertical detachment geometry (VDG), i.e., cuts through the Cu(CD₃OD) potential based on the minimum energy configuration of the anion. For example, the anion surface is

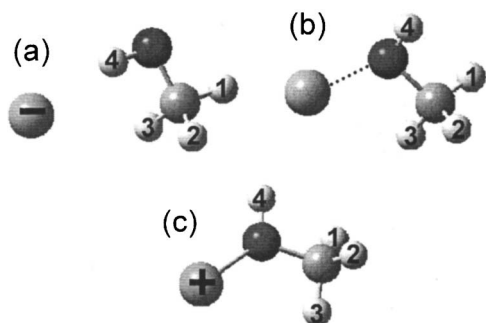


FIG. 3. Minimum energy structures of $\text{Cu}(\text{CD}_3\text{OD})$ complexes for the three charge states of Cu, where (a) shows the structure of the anion, (b) the neutral, and (c) the cation.

calculated as a function of the Cu–O distance R ranging from 1.6–7.6 Å in increments of 0.1 Å. The neutral surface is calculated over a range of 1.5–7.0 Å while the VDG surface ranges from 1.8–7.2 Å; both are evaluated in increments of 0.2 Å. In all scans the O–D bond length and the angle between the plane containing Cu, C, and O and the plane containing D₄, C, and O are relaxed at every step, while all other bond lengths and angles are held constant.

Three types of angular scans were carried out, and the molecular coordinates for these one-dimensional surfaces are based on the structures shown in Fig. 3. The electronic energy is calculated as a function of out-of-plane (OOP) motion by varying the angle between the plane that contains the Cu, O, and C atoms and the plane that contains the D₄, O, and C atoms. This dihedral angle was sampled over a range of $\pm 60^\circ$ for the anion and $\pm 180^\circ$ for the flatter, neutral and VDG surfaces. For all three surfaces, the OOP motion is evaluated in increments of 2° , and the O–D and Cu–O distances are allowed to relax at each step along the path. Variation of the Cu–O–C angle produces in-plane (IP) motion. The electronic energy as a function of this motion is calculated over a $\pm 60^\circ$ range in 2° increments for the anion surface and from -180° to 180° in increments of 10° for the VDG surface; the O–D and Cu–O bond lengths are optimized at each step. For all three complexes, the electronic energy is calculated as a function of methyl torsion (CD_3) over a $\pm 60^\circ$ range of the D₁–C–O–D₄ dihedral angle in 5° increments. In this cut all three C–D bond lengths and O–C–D bond angles are relaxed. The ranges for each of the one-dimensional potentials are chosen such that they span the angular regions sampled by the vibrational wave functions for the states of interest.

B. Vibrational coordinates and Hamiltonian

One-dimensional variational calculations were carried out in a DVR. For the Cu– CD_3OD distance coordinate R , we use the reduced mass of the complex. The effective masses b_{eff} for the angular motions are derived from the rotational constants for the associated molecular motions. In the case of the OOP motion, this corresponds to rotation of the O–D bond about the C–O bond axis. The IP motion corresponds to the rotation of CD_3OD about its C rotation axis coupled to rotation of the complex about its center of mass, while the methyl torsion is simply the threefold rotation of

the CD_3 group about its symmetry axis. Based on the above definitions, the values of b_{eff} for these three motions are 9.9512 cm^{-1} (OOP), 0.6687 cm^{-1} (IP), and 4.5172 cm^{-1} (CD_3), and the effective Hamiltonians for the radial and angular motions are

$$\hat{H} = -\frac{\hbar^2}{2\mu} \frac{d^2}{dR^2} + V(R), \quad (1)$$

$$\hat{H} = b_{\text{eff}} \hat{J}^2 + V(\theta), \quad (2)$$

respectively. Here J^2 is the angular momentum operator associated with the one-dimensional motions, and as such it has eigenvalues that are proportional to j^2 . The potential surfaces V are acquired using spline interpolations of the energies obtained from the electronic structure calculations described above. For the stretch coordinate, grid points used for the DVR calculations range from 0.5 to 15.0 Å with a grid spacing of 0.0181 Å. For the bend and torsion coordinates, the grid ranges from -180° to 180° with a spacing of 0.5° . For the stretch coordinate, grid points beyond those from *ab initio* calculations were necessary, and the *ab initio* data are extrapolated to the calculated value at 25 Å using

$$V_{\text{ex}}(R) = \frac{C_6}{R^6} + \frac{C_8}{R^8}, \quad (3)$$

where the values of C_6 and C_8 are chosen to ensure that the potential and its first derivative are continuous.

Within the Condon approximation, the photoelectron spectrum can be generated from overlaps between eigenstates on the anion and neutral surfaces. Since the low-lying vibrational states on the anion surface are localized near the potential minimum, we focus on those eigenstates on the neutral surface that are evaluated using cuts near the equilibrium structure of the anion, e.g., the VDG surface. Within this treatment, the four-dimensional wave functions are approximated by products of one-dimensional functions. The overlap integrals between the eigenstates on the anion and VDG surfaces are evaluated for each thermally populated state of the anion using the 200 K vibrational temperature as was mentioned above. The resulting spectra are summed and convolved with a Gaussian with a full width at half maximum of 50 cm^{-1} (0.0062 eV). This width is chosen to facilitate comparison with experiment.

IV. RESULTS AND DISCUSSION

A. Initial state characterization

Electron photodetachment from $\text{Cu}^-(\text{CD}_3\text{OD})$ produces an ensemble of neutral $\text{Cu}(\text{CD}_3\text{OD})$ complexes far from their equilibrium geometry, resulting in large amplitude solvent rearrangement and dissociation. In order to investigate the nature of this rearrangement and dissociation, we must characterize the initial state of the ion-molecule complex.

1. Calculations

The anion complex has a distinctly different minimum energy configuration from the neutral and cation complexes. This is illustrated in the variation of selected bond lengths

TABLE I. Select geometrical parameters of all species, calculated at the MP2 level of theory.

	CD ₃ OD	Cu ⁻ (CD ₃ OD)	Cu(CD ₃ OD)	Cu ⁺ (CD ₃ OD)
R(CuO)	...	3.23 Å	2.04 Å	1.86 Å
R(OD)	0.96 Å	0.99 Å	0.96 Å	0.96 Å
R(CO)	1.42 Å	1.41 Å	1.44 Å	1.47 Å
θ _{CO_D}	107.98°	105.82°	108.85°	109.64°

and angles reported in Table I. By analogy to Cu⁻(H₂O), where the Cu⁻ is in a hydrogen-bonded configuration, the minimum energy structure of the Cu⁻(CD₃OD), shown in Fig. 3(a), has the Cu⁻ positioned closest to D₄ and lying in the plane that contains D₄OCD₁. This hydrogen-bonding interaction between Cu⁻ and the OD group in methanol is reflected in the fact that the O–D bond length is 0.03 Å longer in Cu⁻(CD₃OD) than in an isolated methanol molecule. In addition the value of C–O–D angle is decreased from 107.98° in methanol to 105.82° in the cluster. In the context of the present study, the most important change in the methanol by complexation with Cu⁻ is that it lowers the CD₃ torsional barrier by nearly 75%, from 406 cm⁻¹ in an isolated methanol molecule to 110 cm⁻¹ in the complex.

Calculations of the neutral Cu(CD₃OD) cluster at the MP2 level result in a minimum energy structure with the Cu atom closest to the oxygen atom, on the opposite side of the OD group compared to the anion, as shown in Fig. 3(b). In the minimum energy structure, the copper atom resides above the plane that contains D₄OCD₁, and the Cu–O distance is 2.04 Å. In comparing this complex to an isolated methanol molecule, we see that the O–C bond length increases, the O–D bond length remains unchanged, and the C–O–D angle increases slightly. In addition, the barrier to rotation of the methyl group is nearly equal to that in methanol, with a value of 421 cm⁻¹. This change in the barrier height will be important as we analyze the origins of the observed time dependence of the Cu⁺ and Cu⁺(CD₃OD) signals. The large difference between the barrier heights on the anionic and neutral surfaces is surprising, but we have observed similar changes in barrier heights in recent studies of the methyl rotor in CH₃O₂ in its ground and first excited electronic states.⁵¹

Upon electron photodetachment of Cu⁻(CD₃OD), the resulting neutral complex is produced with an initial geometry

TABLE III. Calculated fundamental frequencies for the three vibrational modes corresponding to the 1D potential energy slices of Cu(CD₃OD), minimum energy neutral configuration.

Vibration	15D harmonic (cm ⁻¹)	1D anharmonic (cm ⁻¹)	1D harmonic (cm ⁻¹)
Cu–O stretch	230	183	193
OOP bend	298	246	265
CD ₃ torsion ^a	82	116	123

^aDue to the near degeneracy of the three lowest energy states of the torsion, the 1D values reflect the energy difference between the third excited state and the ground state.

that is close to the minimum energy structure of the anion. Comparing Figs. 3(a) and 3(b), we note that this configuration is far from the minimum energy geometry of the neutral complex. In Tables II and III, we report the harmonic and anharmonic fundamental frequencies of several modes of interest for the anion complex as well as for the two geometries of the neutral complex. The anharmonic frequencies were obtained from the DVR calculations described above, while the one-dimensional harmonic frequencies were obtained by replacing the potential term in Eqs. (1) and (2) with a quadratic expansion of the potential about a local minimum. In contrast the 15-dimensional harmonic frequencies were obtained from a normal mode analysis at the potential minimum. There are obvious differences among the frequencies, and these frequency discrepancies arise from several sources. The differences between the several one-dimensional results reflect the substantial anharmonicity of the potentials. As can be seen, the stretch, IP, and OOP potentials are nearly harmonic, while anharmonicity plays a larger role in the torsion potential. The variation between the two sets of harmonic frequencies reflects the difference between the coordinates that are used to define the one-dimensional potential cuts and the normal mode coordinates.

It should also be noted that no 15-dimensional harmonic calculations are presented for the VDG. This stems from the fact that the vertical detachment geometry is not a stationary point on the neutral surface. However, the VDG manifests itself as local minima in the one-dimensional cuts through the neutral potential energy surfaces. Therefore the one-dimensional calculations are shown in Table II for comparison with the anion and neutral frequencies.

Since the VDG is not the global minimum on the neutral

TABLE II. Calculated fundamental frequencies of the four vibrational modes corresponding to the one-dimensional (1D) potential energy slices for Cu⁻(CD₃OD) and Cu(CD₃OD), which is the neutral complex in the anion configuration, i.e. the vertical detachment geometry.

Vibration	Cu ⁻ (CD ₃ OD)		Cu(CD ₃ OD)		
	15D harmonic (cm ⁻¹)	1D anharmonic (cm ⁻¹)	1D harmonic (cm ⁻¹)	1D anharmonic (cm ⁻¹)	1D harmonic (cm ⁻¹)
Cu–O stretch	138	102	104	54	57
IP bend	83	119	119	24	32
OOP bend	489	423	495	66	212
CD ₃ torsion ^a	44	53	69	105	118

^aDue to the near degeneracy of the three lowest energy states of the torsion, the 1D values reflect the energy difference between the third excited state and the ground state.

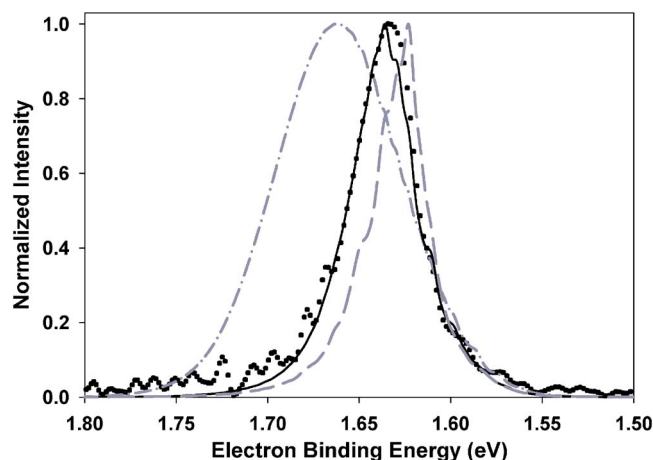


FIG. 4. Experimental and calculated $\text{Cu}^-(\text{CD}_3\text{OD})$ photoelectron spectra. The experimental spectrum is shown as black points. The calculated spectrum is reported with a solid, black curve. For comparison we also calculated the photoelectron spectrum after shifting the potential energy curve for $\text{Cu}^-(\text{CD}_3\text{OD})$ by $\pm 0.18 \text{ \AA}$ along the Cu–O distance coordinate R . The results of these calculations are plotted with gray curves; the dashed line represents the calculation when the potential minimum is shifted to 3.24 \AA and the dash-dot line represents the results when the minimum is at 3.60 \AA .

surface, determining which of the calculated vibrational energy levels correspond to the ground and first excited states of the complex in the VDG can be difficult. For the OOP bend, the lowest energy state that is strongly localized in the VDG minimum is easily assigned, whereas the first excited state is more difficult to isolate. This complication reflects the fact that the barrier to free rotation of the copper atom around the OD group of methanol is only 70 cm^{-1} above this lowest energy state. As the harmonic frequency for this mode is 212 cm^{-1} , it is not surprising that the state that we identify as the first excited state has a frequency much lower than the harmonic value. In fact, its energy is close to the barrier to free rotation, and it is rather delocalized over the full range for the OOP angle. The IP motion also exhibits similar difficulties, albeit to a lesser extent. We also calculated the minimum energy structure of $\text{Cu}^+(\text{CD}_3\text{OD})$, shown in Fig. 3(c); key structural parameters for all three charge states are summarized in Table I.

2. Photoelectron spectra

The $\text{Cu}^-(\text{CD}_3\text{OD})$ photoelectron imaging spectrum reported here was obtained with a pulsed ion machine^{52,53} modified to incorporate a photoelectron imaging device.³⁴ The imaging system is operated in the velocity map imaging^{54,55} mode. This photoelectron imaging spectrometer is very similar to that described by Surber *et al.*⁵⁵ and Mabbs *et al.*⁵⁶ Photoelectrons are accelerated onto a microchannel plate detector coupled to a phosphor screen where images are collected by a charge-coupled device camera. The two-dimensional photoelectron images are reconstructed into the three-dimensional photoelectron velocity and angular distributions using the BASEX image reconstruction method developed by Dribinski *et al.*⁵⁷

The $\text{Cu}^-(\text{CD}_3\text{OD})$ photoelectron spectrum is displayed in Fig. 4.⁵⁸ For comparison, we also plot the calculated $\text{Cu}^-(\text{CD}_3\text{OD})$ photoelectron spectrum, shown as a solid line.

The energy scale of the calculated spectrum has been shifted by 91 meV , such that the maxima of the calculated and experimental spectra coincide. The magnitude and direction of this shift are in line with the error found in our calculation of the electron affinity of Cu atom at the same level of theory.³³

The agreement between the experimental and calculated photoelectron spectra is remarkable. In particular, the calculated spectrum reproduces the width and contour of the experimental spectrum. This provides us with confidence in our reduced dimensional model for the $\text{Cu}(\text{CD}_3\text{OD})$ complex. Analysis of the calculated spectrum shows that its shape and width are captured by a one-dimensional calculation that includes only the Cu–O stretch coordinate, although the methyl rotor motion must also be taken into account to achieve the level of agreement seen in Fig. 4.

While we only report the spectrum that was calculated at 200 K , we also evaluated the photoelectron spectrum for temperatures ranging from 0 to 200 K . The differences among these spectra reflect hot band structure in the Cu–O stretch coordinate and sequence bands in the methyl rotor. The intensities of these features increase with temperature, leading to broadening of the calculated spectrum. Interestingly, the difference between the spectrum at 100 K and that at 200 K are small and are found to be in comparable agreement with the experimental spectrum, shown in Fig. 4. While this insensitivity of the photoelectron spectrum to the vibrational temperature may seem surprising, it reflects the fact that the largest contribution to the width comes from the ground state wave function on the anion surface and is seen at 0 K . Similar behavior was seen in our calculations for $\text{Cu}(\text{H}_2\text{O})$ and $\text{Cu}(\text{D}_2\text{O})$.³³

B. Time evolution of the Cu^+ and $\text{Cu}^+(\text{CD}_3\text{OD})$ signals

The primary focus of this work is the time evolution of $\text{Cu}^+(\text{CD}_3\text{OD})$ and Cu^+ cations that are produced by photodetachment of an electron from $\text{Cu}^-(\text{CD}_3\text{OD})$ followed by two-photon resonant ionization after a specified delay time. The resulting signals, plotted as a function of pump-probe delay time, are reported in Fig. 5.

Before discussing these results, we need to consider how these signals are obtained. Figure 2 displays the photodetachment-photoionization laser schemes superimposed on a schema of the $\text{Cu}(\text{CD}_3\text{OD})$ radial potential energy surface. The Cu^+ signal has primarily a three-color ($398+327+265 \text{ nm}$) dependence, as seen in Fig. 2, scheme 1. The major background in this scheme is produced by a two-color ($327+265 \text{ nm}$) contribution and is typically 10% of the maximum three-color signal. The $\text{Cu}^+(\text{CD}_3\text{OD})$ signal has primarily a two-color ($398+327 \text{ nm}$) dependence, as seen in Fig. 2, scheme 2. As in the $\text{Cu}(\text{H}_2\text{O})_n$ experiments,^{20,21} background measurements indicate that the $398 \text{ nm} + (2 \times 327 \text{ nm})$ contribution to the $\text{Cu}^+(\text{CD}_3\text{OD})$ signal is much larger ($>90\%$) than the $398+327+265 \text{ nm}$ component. One-color backgrounds from both the 398 and 327 nm pulses contribute to both the $\text{Cu}^+(\text{H}_2\text{O})$ and $\text{Cu}^+(\text{CD}_3\text{OD})$ signals.

Figure 5 shows the initial rise of the Cu^+ and $\text{Cu}^+(\text{CD}_3\text{OD})$ signals from $\text{Cu}^-(\text{CD}_3\text{OD})$ following pump

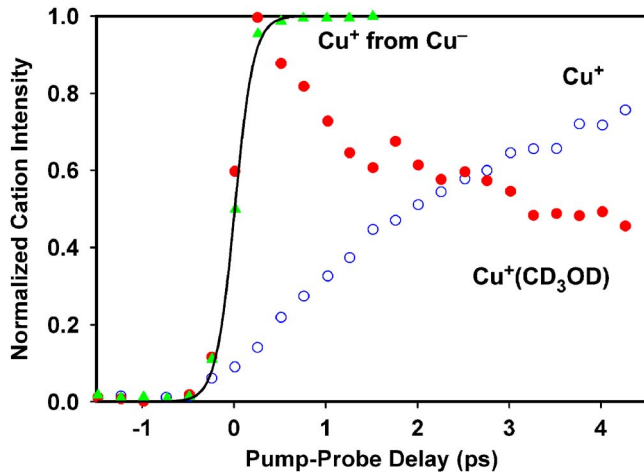


FIG. 5. (Color online) Initial experimental time dependence of cation signals. The Cu⁺ signal rise from Cu⁻ (gray triangles) is fitted with a tanh function (solid line) and used as an *in situ* measure of the instrument time resolution. The open circles represent Cu⁺ signal from Cu(CD₃OD), while the filled circles represent the Cu⁺(CD₃OD) signal from Cu(CD₃OD).

and probe pulses. As a point of reference, the instrument response, measured by the rise of Cu⁺ from Cu⁻, is plotted with gray triangles and fitted with a solid line. The Cu⁺(CD₃OD) signal rises at the same rate as the instrument response while the Cu⁺ signal rises with increasing pump-probe delay. A longer time scan is plotted in Fig. 6. This plot shows that both signals reach their respective asymptotic values by $\sim t=100$ ps. If we sum these two signals, we find that their sum is nearly constant. Similar rise and decay features were also observed in the Cu(H₂O) studies.^{20,21,33}

In order to extract dynamical information from the experimental data, all data sets are summed to produce total Cu⁺ and Cu⁺(CD₃OD) time-dependent signals. Due to day-to-day fluctuations in measured cation intensities as well as in the position of $t=0$, special care needs to be taken when adding multiple data sets. The following procedure is used to

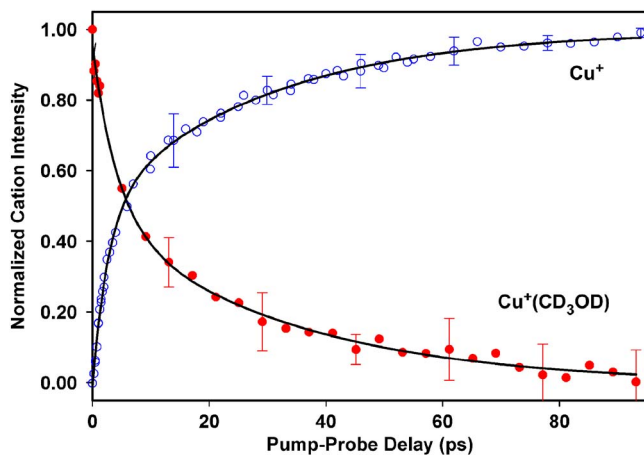


FIG. 6. (Color online) Experimental time dependence of cation signals resulting from photodetachment-photoionization of Cu⁻(CD₃OD). The rising Cu⁺ signal (open circles) results from photodetachment (398 nm) followed by two-color (327+265 nm) resonant ionization. The decaying Cu⁺(CD₃OD) signal (filled circles) results from photodetachment (398 nm) followed by one-color (265 nm) resonant multiphoton ionization. The solid lines represent the exponential fits to the data used to extract time components.

TABLE IV. Parameters of double exponential fit to the functions given in Eqs. (4) and (5); the indicated errors are $\pm 1\sigma$ of the least squares fit parameters.

Cu ⁺	Cu ⁺ (CD ₃ OD)
$x_1=2.9\pm 0.7$ ps	$y_1=5\pm 3$ ps
$x_2=29\pm 4$ ps	$y_2=33\pm 3$ ps
$a_1=0.48\pm 0.10$	$b_1=0.52\pm 0.07$
$a_2=0.52\pm 0.08$	$b_2=0.48\pm 0.08$

account for these fluctuations. First, time-independent background signals are obtained at the beginning and end of each data set. If the background signals changed significantly before and after a data set, then that data set was rejected. For the accepted sets, the average background signal is subtracted from the data set. For the Cu⁺ channel this background correction shows that the $t<0$ signal is zero, while for the Cu⁺(CD₃OD) channel, the background correction shows that the signal is zero both for $t<0$ and for $t>100$ ps. The uncertainty in the determination of $t=0$ is ± 0.25 ps. The complementary shapes of the two curves permits a simple multiplicative scaling of the Cu⁺(CD₃OD) channel intensity, such that the sum of the Cu⁺ and Cu⁺(CD₃OD) signals is essentially constant at a value of 1 for all delay times greater than a few picoseconds. The individual scaled and background-corrected data sets are averaged to obtain the Cu⁺ and Cu⁺(CD₃OD) data shown in Fig. 6. Each data point is an average of $\sim 1.5 \times 10^5$ laser shots. Fitting of the data to single-exponential rise [Cu⁺] and decay [Cu⁺(CD₃OD)] does not produce a satisfactory fit. Consequently a two-component fit was employed. The solid lines in Fig. 6 were obtained by fitting the data to double-exponential rise/decay of the following form:

$$I[\text{Cu}^+] = a_1(1 - e^{-t/x_1}) + a_2(1 - e^{-t/x_2}), \quad (4)$$

$$I[\text{Cu}^+(\text{CD}_3\text{OD})] = b_1e^{-t/y_1} + b_2e^{-t/y_2}. \quad (5)$$

This parametrization gave a satisfactory fit; the parameters so obtained are reported given in Table IV. Although the fits to the Cu⁺ and Cu⁺(CD₃OD) data were carried out independently, the corresponding derived parameters (a_1, b_1), (a_2, b_2), (x_1, y_1), and (x_2, y_2) are each within 1σ of their counterpart. This agreement strongly suggests that both Cu⁺ and Cu⁺(CD₃OD) signals arise from a common physical process. The fitted parameters also show that each component has roughly 50% contribution to the signal. The reported error in fitting is determined by the standard deviation of the exponential fit to the averaged data sets. These errors are represented graphically in Fig. 6 and numerically in Table IV. The large uncertainty present in y_1 comes from the recurring oscillatory features present in the decaying signal, as can be seen in Fig. 5.

C. Dissociation time components

In contrast to the present work, we found that three time scales were required to fit the Cu⁺ signal in the Cu(H₂O) study and that the Cu⁺(H₂O) signal displayed more structure than was observed for Cu⁺(CD₃OD).²⁰ In Cu(H₂O) the

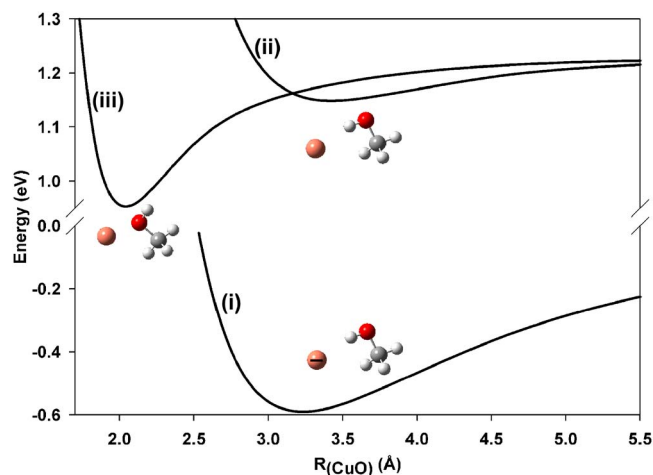


FIG. 7. (Color online) Cuts through the potential energy surfaces along the Cu–O distance coordinate R for (i) $\text{Cu}^-(\text{CD}_3\text{OD})$, (ii) $\text{Cu}(\text{CD}_3\text{OD})$ with other coordinates frozen at the anion configuration, and (iii) fully relaxed $\text{Cu}(\text{CD}_3\text{OD})$. The insets show the various solvent orientations for the three minima.

shortest time scale was ~ 1 ps. This was shown to correspond to the direct dissociation of the $\text{Cu}(\text{H}_2\text{O})$ complex upon electron photodetachment. An intermediate time scale of ~ 10 ps was associated with coupling between the hindered rotation of H_2O in the complex to the Cu– H_2O dissociation channel. Finally the 100 ps component was attributed to vibrational predissociation driven by states with excitation in the water bend.

1. Direct dissociation

As can be seen in Fig. 7, after photodetachment the neutral $\text{Cu}(\text{CD}_3\text{OD})$ complex is in the VDG, a configuration that is far from the minimum energy configuration on the potential surface. The motions that would take the complex to the minimum energy geometry involve a combination of methanol rotation and a shortening of the Cu–O distance. At the equilibrium Cu–O distance in the VDG of $\text{Cu}(\text{CD}_3\text{OD})$, the potential is relatively flat along the coordinates corresponding to methanol rotation. If there is sufficient energy in the Cu–O stretch coordinate, the complex should have enough time to dissociate before getting trapped near the minimum energy configuration of the complex. This mechanism is responsible for the < 1 ps, fast rise signal for Cu^+ from $\text{Cu}^+(\text{H}_2\text{O})$.

As seen in the results reported in Table IV, the parameters that describe the Cu^+ rise do not contain the fast ($t < 1$ ps) Cu^+ component observed in the $\text{Cu}(\text{H}_2\text{O})$ study.²⁰ This direct dissociation component was also absent in the $\text{Cu}(\text{H}_2\text{O})_2$ rearrangement studies.²¹ To understand this difference between the $\text{Cu}(\text{H}_2\text{O})$ and $\text{Cu}(\text{CD}_3\text{OD})$ dissociation dynamics, we turn to cut through the potentials for the anion and neutral species, plotted in Fig. 8. Here the solid lines represent the potentials for the $\text{Cu}(\text{CD}_3\text{OD})$ complexes, while the dashed lines provide the potentials for the $\text{Cu}(\text{H}_2\text{O})$ complexes. The vertical and horizontal dotted lines represent the equilibrium Cu–O distance on the anionic surface and the dissociation energy of the neutral complexes, respectively. As these plots show, upon photodetachment the

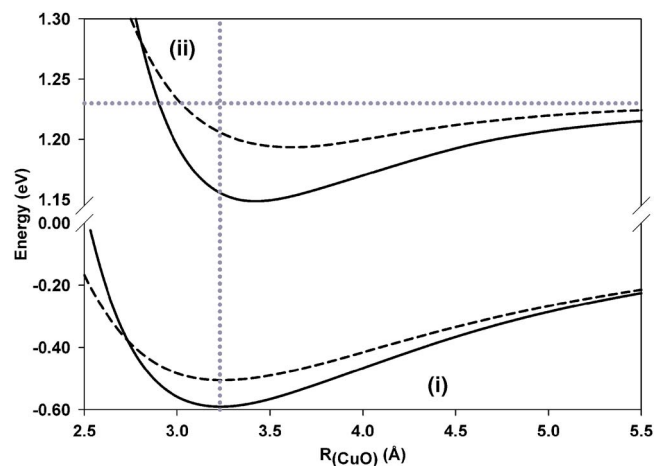


FIG. 8. Cuts through the potential energy surfaces along the Cu–O distance coordinate R for (i) the anion and (ii) the neutral at the vertical detachment geometries of $\text{Cu}(\text{CD}_3\text{OD})$ and $\text{Cu}(\text{H}_2\text{O})$. The solid curves represent $\text{Cu}(\text{CD}_3\text{OD})$, while the dashed curves represent $\text{Cu}(\text{H}_2\text{O})$. The vertical line is drawn at the Cu–O distance corresponding to the minimum energy configuration of both anions. The horizontal line at 1.23 eV indicates the dissociation energy of the neutral complexes.

$\text{Cu}(\text{CD}_3\text{OD})$ complex will be in a configuration that is close to the potential minimum in the VDG along the Cu–O stretch coordinate. Comparison of the well depths shows that the interaction energy of copper in a hydrogen-bonded, Cu– DOCD_3 , orientation with methanol is much larger than the corresponding interaction energy between copper and water in a similar configuration. These differences imply that $\text{Cu}(\text{H}_2\text{O})$ will have more energy along the Cu– H_2O dissociation coordinate than will be the case for $\text{Cu}(\text{CD}_3\text{OD})$.

The implications of the above analysis of the potential curves, plotted in Fig. 8, can be quantified by considering the properties of the ground state wave functions, calculated using the lower, anionic surfaces when they are projected onto the neutral surfaces. If we consider the average energy of these states, we find that it is 148 cm^{-1} below the dissociation threshold [$D_0(C_{2v}) = 265 \text{ cm}^{-1}$] (Ref. 33) in $\text{Cu}(\text{H}_2\text{O})$, while for $\text{Cu}(\text{CD}_3\text{OD})$ the average energy is 568 cm^{-1} below the dissociation threshold ($D_0 = 628 \text{ cm}^{-1}$). While the greater relative energy of $\text{Cu}(\text{H}_2\text{O})$ compared to $\text{Cu}(\text{CD}_3\text{OD})$ supports the above observations, the complexes are initially at a finite temperature, and this should also be taken into account. This can be accomplished by considering the overlaps between the wave functions that correspond to the thermally populated states on the anion surface at 200 K and the vibrational wave functions at the VDG on the neutral surface. We find that 18% of the probability amplitude reflects the overlaps with states with energies above the $\text{Cu}(\text{H}_2\text{O})$ dissociation threshold, while this value drops to less than 2% for $\text{Cu}(\text{CD}_3\text{OD})$. This final observation supports our inability to fit a fast time component, analogous to the < 1 ps rise time in $\text{Cu}(\text{H}_2\text{O})$.

The above arguments rely on the shift between the minimum energy geometries of the slices along the Cu–O coordinate of $\text{Cu}^-(\text{CD}_3\text{OD})$ and $\text{Cu}(\text{CD}_3\text{OD})$ in the VDG. We can investigate the appropriateness of this picture by calculating the photoelectron spectrum, as described above, with the Cu–O distance dependence of the $\text{Cu}^-(\text{CD}_3\text{OD})$ potential

shifted by ± 0.18 Å. The results of these calculations are plotted with dashed lines in Fig. 4. The best agreement in the width of the calculated and experimental spectra is obtained when the calculated vertical detachment potential surface is used. This finding, along with the calculated overlaps between the radial wave functions and the anion and VDG potential energy surfaces, supports the fact that the direct dissociation channel that was reported for the Cu(H₂O) complex is not observed in Cu(CD₃OD).

2. Energy redistribution

While the above discussion shows that there is not enough energy directly deposited into the Cu–O coordinate of Cu(CD₃OD) to lead to direct dissociation, in most cases there is more than sufficient excitation in several of the other vibrational degrees of freedom to dissociate the complex. An investigation of cuts through the neutral potentials, corresponding to both the IP and OOP motions, reveals a relatively flat landscape similar to that seen in Cu(H₂O). In our three-dimensional simulations of the dynamics of Cu(H₂O) on the neutral surface, we were able to attribute the 10 ps time scale obtained from the fits to the Cu⁺ and Cu⁺(H₂O) signals to energy transfer between the hindered rotation of the water molecule and the dissociation coordinate. When we compare the initial internal energy in the IP and OOP rotation coordinates in these two systems, based on one-dimensional calculations, we find that they differ by less than 10%. This, coupled to the similarity of the 3 ps time scale obtained in the present study and the 10 ps time scale for Cu(H₂O), leads us to conclude that the motions responsible for the 3 ps rise and decay times reported in Table IV are associated with energy transfer from the methanol hindered rotation to the dissociation of the complex. The shorter time scale for methanol compared to water likely reflects the smaller rotational constants for methanol leading to a larger density of states.

In the Cu(H₂O) study, the 100 ps dissociation component stemmed from predissociation driven by vibrationally excited bending modes of H₂O. In Table IV we report the longest dissociation component as 30 ps for Cu(CD₃OD). We believe that this component arises from coupling of the methyl rotor rotation into the Cu–CD₃OD dissociation coordinate. When we calculate the overlap between the thermally populated torsional levels of the CD₃ group in Cu[−](CD₃OD) and the states on the neutral surface, we find that, upon photodetachment, 65% of the probability amplitude ends up in states with energy in the methyl torsion. This value is within 2σ of the values for a_2 and b_2 , reported in Table IV. Based on this, we attribute the 30 ps time scale to coupling of states with methyl rotor excitation to the dissociation coordinate. We ascribe the difference in the dissociation time, compared to the 100 ps component of Cu(H₂O), to the presence of the methyl rotor and its ability to accelerate intramolecular vibrational energy redistribution.^{59–61}

V. CONCLUSIONS

We report the experimental and theoretical investigations of the time-dependent dissociation dynamics of the

Cu(CD₃OD) complex. Experiments using photodetachment-photoionization spectroscopy provide insight into the evolution of the nascent neutral complex formed via electron photodetachment from Cu[−](CD₃OD). *Ab initio* calculations provide the minimum energy structures and one-dimensional potential energy surfaces used in determining the vibrational energies and wave functions of the complex.

The *ab initio* minimum energy structures show that both Cu(H₂O) and Cu(CD₃OD) have similar hydrogen-bonded anion orientations as well as similar neutral Cu–O orientations. However, the Cu(CD₃OD) complex does not exhibit the direct dissociation ($t < 1$ ps) observed in Cu(H₂O), due to the predominantly bound-to-bound transitions upon electron photodetachment of Cu[−](CD₃OD). The rising Cu⁺ and decaying Cu⁺(CD₃OD) signals from Cu(CD₃OD) both exhibit time components of 3 and 30 ps. Models of the dissociation dynamics suggest that the 3 ps component arises from coupling of CD₃OD hindered rotations to the Cu–CD₃OD dissociation coordinate; this time scale is comparable to the solvent reorientation coupling observed in Cu(H₂O). The angular one-dimensional potential energy slices and calculated excitation energies confirm the similarity of the two systems in the solvent reorientation coordinates. Further modeling of the dynamics suggests that the excited methyl rotations couple into the Cu–CD₃OD dissociation coordinate on a 30 ps time scale, slightly faster than the 100 ps time scale observed in Cu(H₂O).

ACKNOWLEDGMENTS

One of the authors (A.B.M.) gratefully acknowledge support from NSF Grant No. CHE0515627, another author (W.C.L.) from NSF Grant Nos. CHE0512188 and PHY0551010, and (W.C.L.) from AFOSR Grant No. FA9550-06-1-006. Another author (J.B.) was partially supported by the Optical Science and Engineering Program (IG-ERT) at the University of Colorado. The electronic structure calculations were performed on the JILA Keck cluster, for which the authors acknowledge support from the W. M. Keck Foundation. They would also like to acknowledge Dr. Django Andrews for obtaining the Cu[−](CD₃OD) photoelectron spectrum reported here.

¹M. A. Duncan, *Annu. Rev. Phys. Chem.* **48**, 69 (1997).

²M. A. Duncan, *Int. Rev. Phys. Chem.* **22**, 407 (2003).

³W. H. Robertson and M. A. Johnson, *Annu. Rev. Phys. Chem.* **54**, 173 (2003).

⁴J. R. Roscioli, E. G. Diken, M. A. Johnson, S. Horvath, and A. B. McCoy, *J. Phys. Chem. A* **110**, 4943 (2006).

⁵H. Schneider, A. D. Boese, and J. M. Weber, *J. Chem. Phys.* **123**, 084307 (2005).

⁶A. D. Boese, H. Schneider, A. N. Gloss, and J. M. Weber, *J. Chem. Phys.* **122**, 154301 (2005).

⁷J. M. Weber and H. Schneider, *J. Chem. Phys.* **122**, 069901 (2005).

⁸E. G. Diken, G. H. Weddle, J. M. Headrick, J. M. Weber, and M. A. Johnson, *J. Phys. Chem. A* **108**, 10116 (2004).

⁹T. E. Dermota, Q. Zhong, and A. W. Castleman, *Chem. Rev. (Washington, D.C.)* **104**, 1861 (2004).

¹⁰D. M. Neumark, *Annu. Rev. Phys. Chem.* **52**, 255 (2001).

¹¹R. Parson, N. Delaney, A. Sanov, and W. C. Lineberger, in *Physics and Chemistry of Clusters*, Proceedings of Nobel Symposium 117, edited by E. E. B. Campbell and M. Larsson (World Scientific, Singapore, 2001), p. 132.

¹²A. Sanov and W. C. Lineberger, *PhysChemComm* **5**, 165 (2002).

- ¹³ Q. Zhong and A. W. Castleman, Jr., *Chem. Rev. (Washington, D.C.)* **100**, 4039 (2000).
- ¹⁴ D. M. Neumark, *J. Chem. Phys.* **125**, 132303 (2006).
- ¹⁵ C. P. Schulz, A. Gerber, C. Nitsch, and I. V. Hertel, *Z. Phys. D: At., Mol. Clusters* **20**, 65 (1991).
- ¹⁶ C. P. Schulz, J. Hohndorf, P. Brockhaus, F. Noack, and I. V. Hertel, in *Structures and Dynamics of Clusters*, edited by T. Kondow, K. Kaya Keio, and A. Terasaki (Universal Academic, Tokyo, 1996), Vol. 16, p. 191.
- ¹⁷ C. P. Schulz and C. Nitsch, *J. Chem. Phys.* **107**, 9794 (1997).
- ¹⁸ C. P. Schulz, A. Scholz, and I. V. Hertel, *Springer Ser. Chem. Phys.* **63**, 621 (1998).
- ¹⁹ C. P. Schulz, A. Scholz, and I. V. Hertel, *Isr. J. Chem.* **44**, 19 (2004).
- ²⁰ F. Muntean, M. S. Taylor, A. B. McCoy, and W. C. Lineberger, *J. Chem. Phys.* **121**, 5676 (2004).
- ²¹ M. S. Taylor, J. Barbera, C. P. Schulz, F. Muntean, A. B. McCoy, and W. C. Lineberger, *J. Chem. Phys.* **122**, 054310 (2005).
- ²² S. E. Bradforth and P. Jungwirth, *J. Phys. Chem. A* **106**, 1286 (2002).
- ²³ G. M. Chaban, S. S. Xantheas, and R. B. Gerber, *J. Phys. Chem. A* **107**, 4952 (2003).
- ²⁴ D. D. Kemp and M. S. Gordon, *J. Phys. Chem. A* **109**, 7688 (2005).
- ²⁵ M. Meot-Ner, *Chem. Rev. (Washington, D.C.)* **105**, 213 (2005).
- ²⁶ J. L. Rheinecker and J. M. Bowman, *J. Chem. Phys.* **124**, 131102 (2006).
- ²⁷ M. Roeselová, U. Kaidor, and P. Jungwirth, *J. Phys. Chem. A* **104**, 6523 (2000).
- ²⁸ M. Roeselová, M. Mucha, B. Schmidt, and P. Jungwirth, *J. Phys. Chem. A* **106**, 12229 (2002).
- ²⁹ D. E. Szpunar, K. E. Kautzman, A. E. Faulhaber, and D. M. Neumark, *J. Chem. Phys.* **124**, 054318 (2006).
- ³⁰ J. R. Verlet, A. Kammrath, G. B. Griffin, and D. M. Neumark, *J. Chem. Phys.* **123**, 231102 (2005).
- ³¹ S. S. Xantheas, *J. Phys. Chem.* **100**, 9703 (1996).
- ³² S. Kondo, K. Hashimoto, and H. Tachikawa, *Chem. Phys. Lett.* **431**, 45 (2006).
- ³³ M. S. Taylor, F. Muntean, W. C. Lineberger, and A. B. McCoy, *J. Chem. Phys.* **121**, 5688 (2004).
- ³⁴ G. J. Rathbone, T. Sanford, D. Andrews, and W. C. Lineberger, *Chem. Phys. Lett.* **401**, 570 (2004).
- ³⁵ G. Caldwell and P. Kebarle, *J. Am. Chem. Soc.* **106**, 967 (1984).
- ³⁶ T. D. Fridgen, T. B. McMahon, P. Maitre, and J. Lemaire, *Phys. Chem. Chem. Phys.* **8**, 2483 (2006).
- ³⁷ D. W. Boo, Y. Ozaki, L. H. Andersen, and W. C. Lineberger, *J. Phys. Chem. A* **101**, 6688 (1997).
- ³⁸ W. H. Robertson, J. A. Kelley, and M. A. Johnson, *Rev. Sci. Instrum.* **71**, 4431 (2000).
- ³⁹ P. J. Campagnola, L. A. Posey, and M. A. Johnson, *J. Chem. Phys.* **95**, 7998 (1991).
- ⁴⁰ J. M. Papanikolas, J. R. Gord, N. E. Levinger, D. Ray, V. Vorsa, and W. C. Lineberger, *J. Phys. Chem.* **95**, 8028 (1991).
- ⁴¹ W. C. Wiley and I. H. McLaren, *J. Mass Spectrom.* **32**, 4 (1997).
- ⁴² V. Vorsa, P. J. Campagnola, S. Nandi, M. Larsson, and W. C. Lineberger, *J. Chem. Phys.* **105**, 2298 (1996).
- ⁴³ Z. Bacic and J. C. Light, *Annu. Rev. Phys. Chem.* **40**, 469 (1989).
- ⁴⁴ D. T. Colbert and W. H. Miller, *J. Chem. Phys.* **96**, 1982 (1992).
- ⁴⁵ M. J. Frisch, G. W. Trucks, H. B. Schlegel *et al.*, GAUSSIAN 98, Gaussian, Inc., Pittsburgh, PA, 1998.
- ⁴⁶ M. J. Frisch, G. W. Trucks, H. B. Schlegel *et al.*, GAUSSIAN 03 Gaussian, Inc., Pittsburgh, PA, 2003.
- ⁴⁷ M. Dolg, U. Wedig, H. Stoll, and H. Preuss, *J. Chem. Phys.* **86**, 866 (1987).
- ⁴⁸ X.-B. Wang, L.-S. Wang, R. Brown, P. Schwerdtfeger, D. Schröder, and H. Schwarz, *J. Chem. Phys.* **114**, 7388 (2001).
- ⁴⁹ R. A. Kendall, T. H. Dunning, Jr., and R. J. Harrison, *J. Chem. Phys.* **96**, 6796 (1992).
- ⁵⁰ T. H. Dunning, Jr., *J. Chem. Phys.* **90**, 1007 (1989).
- ⁵¹ G. M. P. Just, T. A. Miller, and A. B. McCoy (unpublished).
- ⁵² M. E. Nadal, P. D. Kleiber, and W. C. Lineberger, *J. Chem. Phys.* **105**, 504 (1996).
- ⁵³ A. Sanov, T. Sanford, S. Nandi, and W. C. Lineberger, *J. Chem. Phys.* **111**, 664 (1999).
- ⁵⁴ A. Eppink and D. H. Parker, *Rev. Sci. Instrum.* **68**, 3477 (1997).
- ⁵⁵ E. Surber, R. Mabbs, and A. Sanov, *J. Phys. Chem. A* **107**, 8215 (2003).
- ⁵⁶ R. Mabbs, K. Pichugin, E. Surber, and A. Sanov, *J. Chem. Phys.* **121**, 265 (2004).
- ⁵⁷ V. Dribinski, A. Ossadtchi, V. Mandelshtam, and H. Reisler, *Rev. Sci. Instrum.* **73**, 2634 (2002).
- ⁵⁸ D. H. Andrews, Ph.D. thesis, University of Colorado, 2006.
- ⁵⁹ D. B. Moss and C. S. Parmenter, *J. Chem. Phys.* **98**, 6897 (1993).
- ⁶⁰ C. S. Parmenter and B. M. Stone, *J. Chem. Phys.* **84**, 4710 (1986).
- ⁶¹ P. J. Timbers, C. S. Parmenter, and D. B. Moss, *J. Chem. Phys.* **100**, 1028 (1994).